UNIVERSITY OF WASHINGTON

A Simulation of the ATLAS Muon Detector End-Cap Alignment Bar Deformation Model

Craig Dowell[†]

University of Washington, Seattle, WA

Abstract

The Large Hadron Collider (LHC) at the European Organization for Nuclear Research (CERN) is a particle accelerator due to switch on in 2007. The end-cap muon spectrometers of the ATLAS detector are arranged in "wheels." The positions of these wheels must be accurately known to approximately 30-50 μm to achieve the desired detector accuracy. An alignment system was developed based on a reference bar concept to enable this precision. Kinematically mounted reference rulers, called alignment bars, allow for prediction of the shape of the system based on a theoretical model. In tests conducted on an octant of a prototype end-cap wheel at the LHC test beam, somewhat surprising results were seen in the shape of the alignment bars during relatively fast changes in temperature. It has been hypothesized that friction and a resulting torque in the kinematic mounting system of the alignment bars gives rise to the deformations. This paper describes a simple mathematical model that was developed to describe the deformations, and compares the output of the model with the data gathered at the CERN test beam.

[†] Email comments or questions to: craigdo@u.washington.edu

1. INTRODUCTION

The Large Hadron Collider (LHC) is a particle accelerator located at the European Organization for Nuclear Research (CERN). It is being built in a circular tunnel (see Figure 1) 27 kilometers in circumference, buried from 50 to 175 meters underground. It is designed to collide two beams of counter-rotating protons at energies of around 7 TeV (tera electron volts. 1 TeV = 10^{12} eV).

Figure 1: The LHC Tunnel

When the particles collide, they do so in a detector. The ATLAS (A large Toroidal LHC ApparatuS) detector is the heart of the experiment that will explore the fundamental nature of matter and the four fundamental forces of the universe. The detector is shown schematically in Figure 2. If you look closely at the bottom of the image, you can see two people shown to scale. The detector is about the size of a five story building.

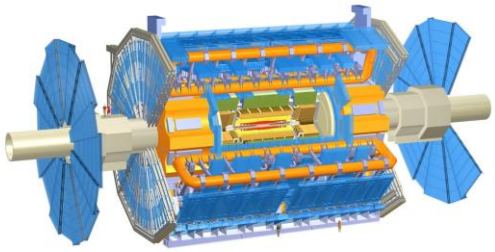

Figure 2: The ATLAS Detector

The ATLAS detector is composed of 1) an inner detector that measures the directions, momenta, and signs of charge of electrically-charged particles produced in a proton-proton collision; 2) an electromagnetic calorimeter that measures the energies of the electrons and photons; 3) an hadronic calorimeter that measures the energies of the hadrons (protons, neutrons, pions – heavy particles made of quarks); and 4) the muon system.

The muon system is also composed of a number of different types of sensors. The muon portion of the ATLAS detector is shown in Figure 3 (in blue). The end-cap spectrometers are the wheel-shaped structures at both ends of the detector. These are the structures which concern us in this paper.

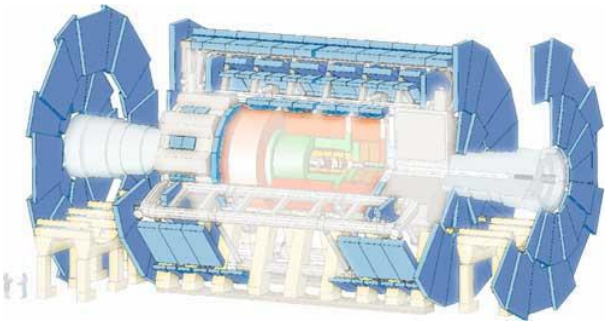

Figure 3: The Muon System

The physical detectors in the muon end-cap spectrometers are mounted to precisely aligned frames, an example of which is shown in Figure 4.

Figure 4: An End-Cap Spectrometer Frame

In order to achieve the required measurement precision, an alignment system is added that allows for the precise reconstruction of the geometry of the spectrometer system as a whole. A portion of the basic alignment system is shown schematically in Figure 5.

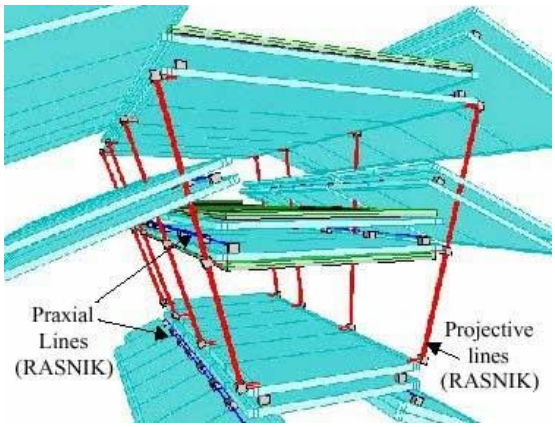

Figure 5: A Portion of the Muon Detector Alignment System

The devices which measure distances between components of the alignment system are called RasNIK (Relative alignment system of NIKHEF) devices. Temperature sensors are collocated with the RasNIKs to allow prediction of length changes due to thermal expansion. Although the complete system is not up and running, a (relatively) small prototype has been operating for some time, gathering data.

Of particular interest to us are the alignment bars. The alignment bars act as precision reference rulers and allow the geometry of the detector to be determined to the desired precision. Alignment bars are instrumented aluminum cylinders. The instrumentation includes eight temperature probes distributed along the length of the bar, and four independent RasNIK systems. The instrumentation results and an analytical bar shape model are combined to predict a bar shape that is extremely accurate. The design for the prototypical alignment bar is shown in Figure 6.

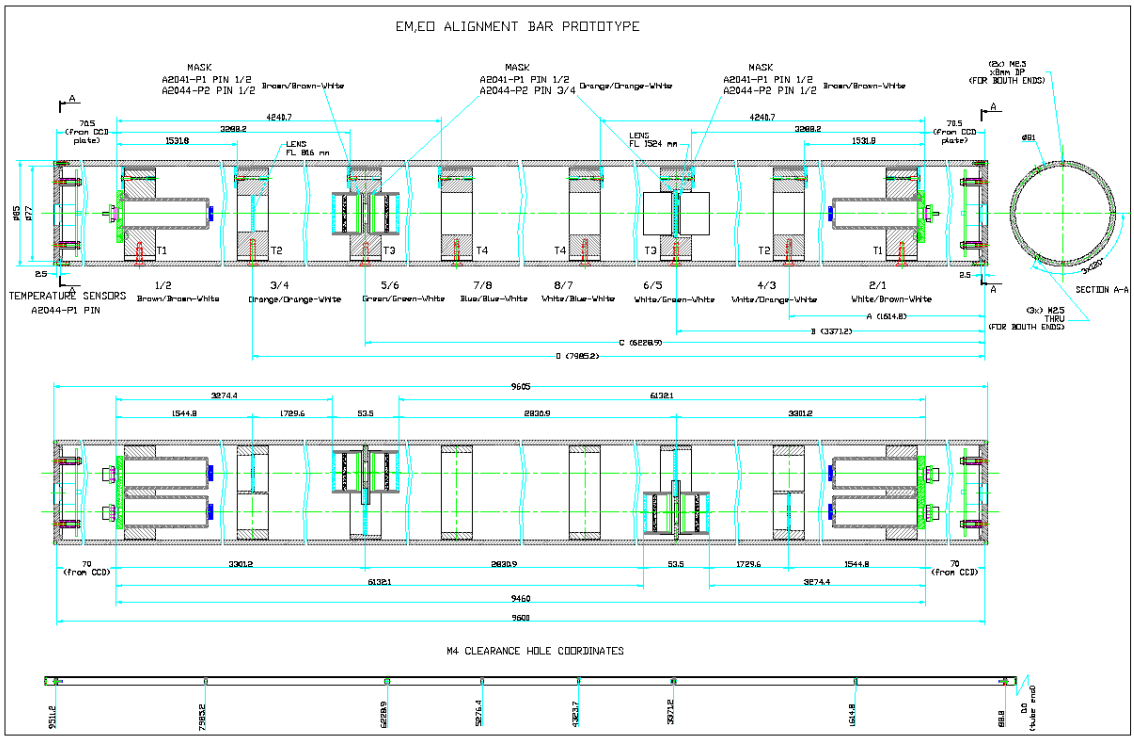

Figure 6: The Design of a Prototypical Alignment Bar

Alignment bars are mounted kinematically and supported at two points. A kinematic mounting ensures that all six degrees of freedom[2] (DOF) are singly constrained (so that the bar does not move), but at the same time ensures that no stress is introduced by overconstraining any degree of freedom. The alignment bar in the test beam is fixed in position on one side by a gimbal as shown in Figure 7 (Left). The other side is constrained by the simplified loose bearing shown in Figure 7 (Right). This bearing allows the alignment bar to slide (along a track to which the bearing is mounted) in the z

[2] Linear translation along the x-, y- and z-axis; and rotation around the x-, y- and z-axis.

direction as it expands and contracts in response to ambient temperature changes. You can see that great care was taken to ensure that an alignment bar would be free to expand and contract according to temperature variations.

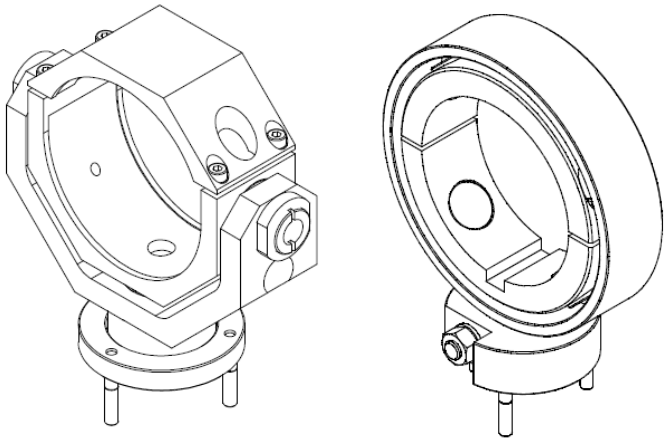

Figure 7: Left: Gimbal Mount Permitting Two Degrees of Freedom (rotation about the x- and y-axes); Right: Simplified Loose Bearing Permitting Four Degrees of Freedom (rotation about the x-, y-, and z-axes and linear motion in the z direction).

The RasNIK devices inside the alignment bars measure bar distortion in the x- and y-axis very accurately (on the order of 10 μm). They measure length in the z-axis somewhat less accurately (to perhaps 50 μm). They do this by projecting an image of a very fine grid (a coded mask) onto a distant CCD camera. This is shown schematically in Figure 8.

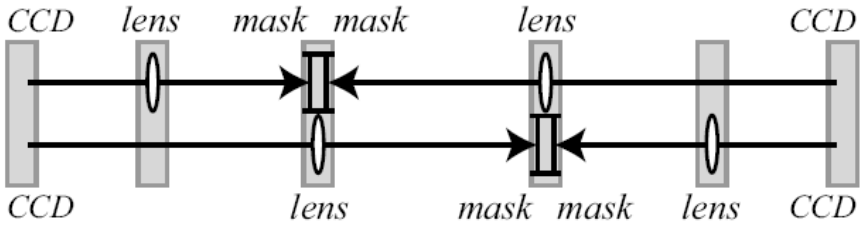

Figure 8: The Design of a RasNIK Measurement System

As the ends of the alignment bar move in the x-y plane, the image of the mask on the CCD camera is translated linearly. As the length of the alignment bar changes, the apparent magnification of the mask image changes. The RasNIK software detects these image changes and reports them as relative movement in x and y (reported in millimeters, with precision to the μm level), and a magnification value (with corresponding precision).

Figure 9 shows how to interpret the measurements. The left half of the diagram reflects a short RasNIK system. There is a mask at the center line which is projected to the left, through a lens, to a CCD located at the left side of the diagram. If an alignment bar containing this instrument was to bow upward, as the shape of the left half of the curve indicates (with respect to the straight line from the CCD to the center lens) the CCD at the far left would end up seeing a different area of the mask that it would if the optics

were aligned along the horizontal axis. Since the image of the projected mask is inverted, an upward bow results in the CCD seeing a view of a lower portion of the mask. This is reported as a lower number in the coordinate axis.

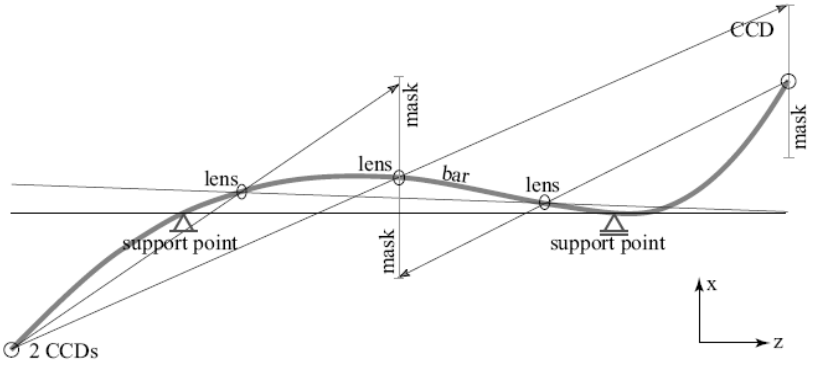

Figure 9: Interpretation of Measurements Provided by a RasNIK

Based on the kinematic mounting of the alignment bars, its designers expected that there would be very little shape distortion of an alignment bar as the temperature varied. It was expected that, as the alignment bar expanded, the simplified loose bearing would slide smoothly, not constraining the motion of the bar. The intention was that the bar shape model could predict the length of the alignment bar very accurately from the material's coefficient of linear thermal expansion, and they anticipated a very small torque due to the lever arm of the bearing, but calculated that it would be negligible. The designers were somewhat surprised to see the results shown in Figure 10.

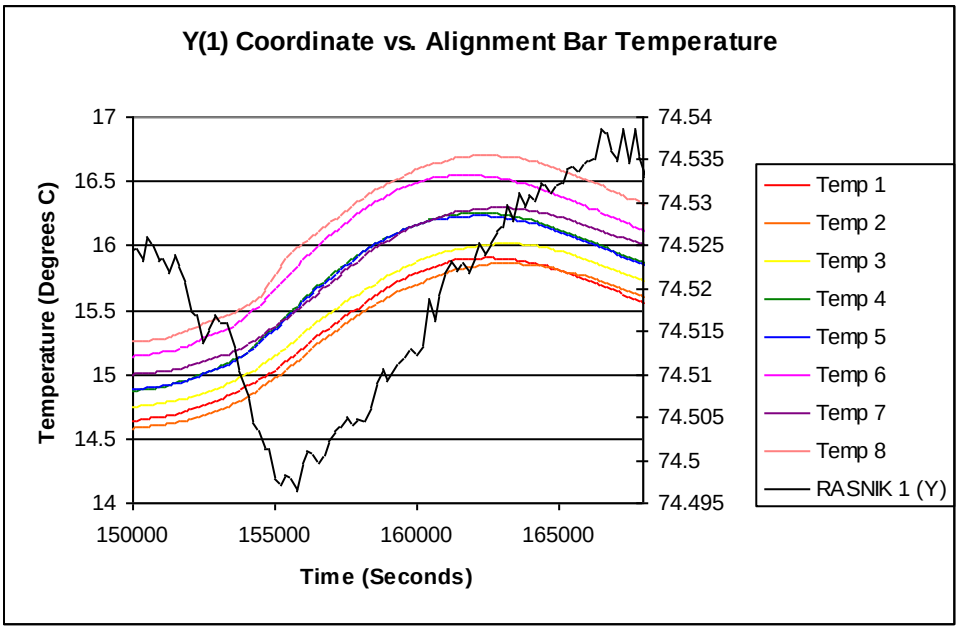

Figure 10: Alignment Bar Distortion and Temperature Versus Time. Data Collected from CERN Test Beam

In Figure 10, as the temperature begins to increase quickly (there are eight temperature readings in the plot), a bow in the alignment bar appears. This is reflected in the RasNIK reading decreasing from about 74.525 mm to a little over 74.495 mm. This is a maximum deflection of 30 μm that is roughly correlated with the negative derivative of temperature.

It has since been hypothesized that an unexpectedly large torque due to friction in the simplified bearing mount is the cause of the distortion. The model described in this paper was developed to determine the validity of this hypothesis.

2. IDENTIFICATION

The basic question to be answered by evaluation of the model developed for this project is, “does thermal expansion of the alignment bar, resisted by the friction of the simplified loose bearing mount, combined with the effects of a resulting torque due to the off-center action of the friction force, explain the surprising deformation found at the CERN test beam”?

3. ASSUMPTIONS AND SIMPLIFICATIONS

The alignment bar is modeled as a cylindrical spring with an 80 mm outer diameter and a 72 mm inner diameter. The material is Anticorodal 6004 thermal treated aluminum with an intrinsic straightness $\leq$ 1 mm/m. An available value for Young's modulus is used to create an effective spring force for the aluminum tube. The thermal expansion characteristics for the tube are assumed to be linear, proportional to the coefficient of linear expansion of the aluminum material. Expansion is assumed to be negligible in all but the longitudinal axis of the cylinder. Temperature gradients are assumed to be negligible and a single relative temperature change value is used to determine the overall linear expansion of the bar.

The bar is assumed to be a free-body with the exception of the constraining force to be investigated. This means that all six degrees of freedom are singly constrained in order to fix the bar's position in space, and no stress is introduced except that due to the single imposed constraint. The effects of gravity on the shape of the alignment bar as it expands and contracts are assumed to be negligible.

Tunable parameters for two types of damping force are defined for the model: viscous damping and Coulomb friction. Although Coulomb friction is probably a more realistic type of friction force (not proportional to velocity), viscous damping is an alternative mechanism and will also be investigated, especially since it is proportional to the derivative of velocity.

4. FORMULATION OF THE MODEL

The model is a single degree-of-freedom (SDOF) model, which is described by a single second-order differential equation. A free-body diagram was generated to aid in visualizing the forces affecting the alignment bar.

Figure 11 shows the free-body diagram in its conventional orientation. The alignment bar is modeled as the spring. The "wall" to the left of the diagram corresponds to the gimbal mount which constrains the end of the alignment bar. In this simplified model, only the longitudinal axis of the alignment bar is represented. In order to follow convention, we call this axis the x-axis. The force, F_s, is the spring force of the alignment bar itself, extrapolated from Young's modulus and the dimensions of the bar. This force appears in the model as κ. An imaginary unit mass (actually the last section of the bar itself) at the end of the alignment bar serves as the free-body, represented in grey in Figure 11.

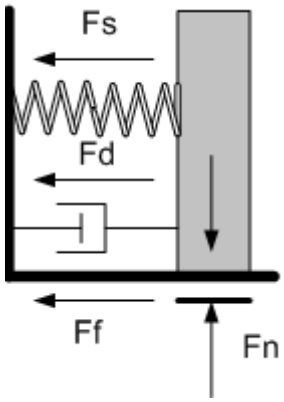

Figure 11: The Free-Body Diagram of the Alignment Bar Model

Any viscous drag on the alignment bar is represented by the dashpot in Figure 11, and is signified by the F_d force vector. Coulomb friction is represented by the normal force "pressing" on a horizontal line below the body. The product of the normal force and the coefficient of kinetic friction yields the friction force signified by the F_f vector.

The equation of motion for the model is derived by applying Newton's second law to the sum of the forces acting in the x direction,

$$ma = \sum F_x \, .$$

The spring force is defined using Hooke's law and acts in the $-x$ direction,

$$F_s = -\kappa x \, .$$

The viscous drag force is proportional to the velocity and acts in the opposite direction,

$$F_d = -\zeta \frac{dx}{dt}.$$

The coulomb friction is proportional to the normal force and acts against movement,

$$F_f = -\mu_k N \cdot \mathrm{sgn}\left(\frac{dx}{dt}\right).$$

For example, if the object is moving in the positive x direction, dx/dt is positive and the force is a negative constant force over velocity.

Substituting these values into Newton's second law, we find,

$$m\frac{d^2x}{dx^2} = -\kappa x - \zeta \frac{dx}{dt} - \mu_k N \cdot \mathrm{sgn}\left(\frac{dx}{dt}\right),$$

or, equivalently,

$$m\frac{d^2x}{dx^2} + \kappa x + \zeta \frac{dx}{dt} + \mu_k N \cdot \mathrm{sgn}\left(\frac{dx}{dt}\right) = 0.$$

We want to allow for a time-dependent forcing function (the ambient temperature), so we can write,

$$m\frac{d^2x}{dx^2} + \kappa x + \zeta \frac{dx}{dt} + \mu_k N \cdot \mathrm{sgn}\left(\frac{dx}{dt}\right) = f(t). \qquad (1)$$

This is a second-order ordinary non-homogenous linear differential equation if the coefficient of kinetic friction is zero. If we include Coulomb friction, the equation becomes non-linear due to the discontinuity of the sgn() function – however it can be solved piecewise.

Equation (1) is the equation of motion for the modeled alignment bar.

5. SOLUTION AND VERIFICATION OF THE MODEL

In order to verify that equation (1) is providing the expected results, I used Maple to generate various solutions of increasing complexity and verified the results, primarily qualitatively. In all cases, I assume the object representing the end of the alignment bar has unit mass. The first solution sets $\zeta = 0,\ \mu_k = 0,\ \kappa = 0,\ f(t) = t$. This corresponds to a force applied to an object on a frictionless surface. Figure 12 shows the results of this test.

```
> ode:= diff(diff(x(t),t),t) + (zeta)*diff(x(t),t) +
(kappa)*x(t) + mu*N = F(t);
```

$$ode := \frac{\partial^2}{\partial t^2} x(t) = t$$

```
> dsolve(ode);
```

$$x(t) = \frac{1}{6} t^3 + \_C1\, t + \_C2$$

```
> dsolve({ode,x(0)=0, D(x)(0)=0});
```

$$x(t) = \frac{1}{6} t^3$$

Figure 12: Maple Code for Force Applied to Object on Frictionless Surface

The solution with the boundary conditions, $x(0) = 0,\ \dot{x}(0) = 0$, is consistent with the expected behavior. Taking two derivatives, we recover $\frac{d^2x}{dx^2} = t$, or $F = ma = t$.

For the next test, I added some Coulombic (kinetic) friction by setting $\mu_k = 1,\ N = 1$.

```
> ode:= diff(diff(x(t),t),t) + (zeta)*diff(x(t),t) +
(kappa)*x(t) + mu*N = F(t);
```

$$ode := \left(\frac{\partial^2}{\partial t^2}\,\mathrm{x}(t)\right) + 1 = t$$

```
> dsolve(ode);
```

$$\mathrm{x}(t) = \frac{1}{6}t^3 - \frac{1}{2}t^2 + \_C1\,t + \_C2$$

```
> dsolve({ode,x(0)=0, D(x)(0)=0});
```

$$\mathrm{x}(t) = \frac{1}{6}t^3 - \frac{1}{2}t^2$$

Figure 13: Maple Code for Force Applied to Object on Frictionful Surface

Figure 13 shows that the solution with the boundary conditions $x(0)=0,\ \dot{x}(0)=0$ is as expected. The position vs. time is reduced due to the friction, and after taking two derivatives, we recover $\frac{d^2x}{dx^2} = t - 1$.

I next modeled an undamped harmonic oscillator by setting the tunable parameters to $\zeta = 0,\ \mu_k = 0,\ \kappa = 1,\ f(t) = 0$.

```
> ode:= diff(diff(x(t),t),t) + (zeta)*diff(x(t),t) +
(kappa)*x(t) + mu*N = F(t);
```

$$ode := \left(\frac{\partial^2}{\partial t^2}\,\mathrm{x}(t)\right) + \mathrm{x}(t) = 0$$

```
> dsolve(ode);
```

$$\mathrm{x}(t) = \_C1\sin(t) + \_C2\cos(t)$$

```
# Initial condition is extending the mass out to x=1 and releasing it
> soln := dsolve({ode,x(0)=1, D(x)(0)=0});
```

$$soln := \mathrm{x}(t) = \cos(t)$$

```
> plot(cos(t), t=0..10);
```

Figure 14: Maple Code for Undamped Harmonic Oscillator

Figure 15 shows the response of the harmonic oscillator to be exactly as expected.

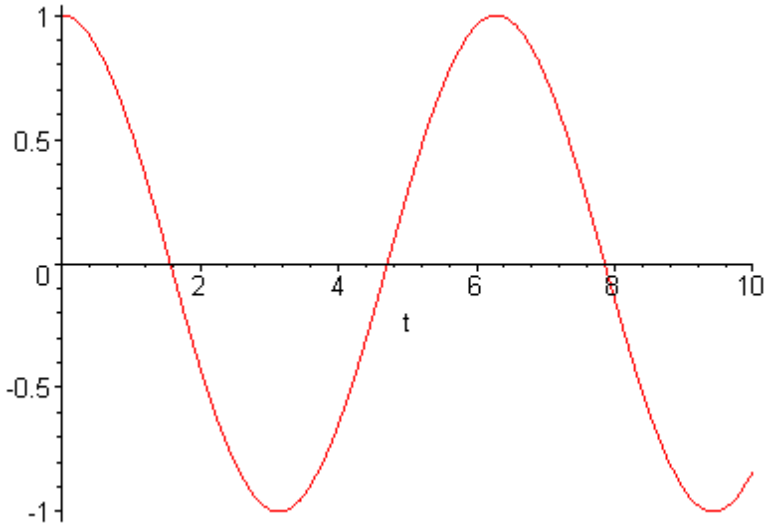

Figure 15: Response of the Undamped Harmonic Oscillator

Similar tests were done to verify a viscously damped harmonic oscillator (Figure 16) and a forced, viscously damped harmonic oscillator (Figure 17).

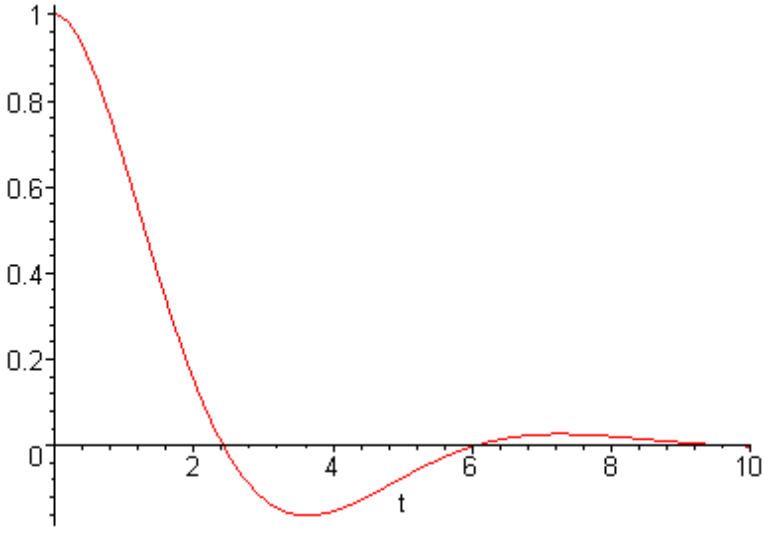

Figure 16: Response of the Viscously Damped Harmonic Oscillator

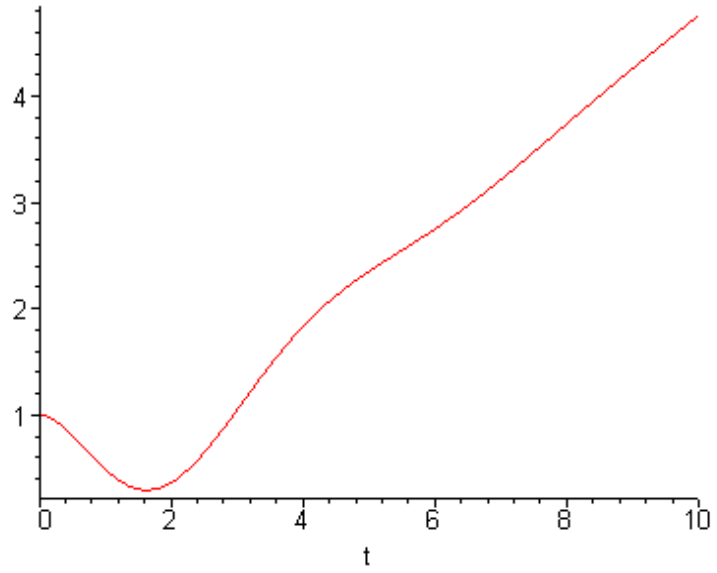

Figure 17: Response of the Driven Viscously Damped Harmonic Oscillator

It was determined that the model is producing appropriate, physically meaningful results.

6. ADAPTING THE SDOF MODEL TO THE ALIGNMENT BAR

Equation (1) is a generic model of the motion of a free body under SDOF constraints. The alignment bar expands and contracts based on its surrounding temperature, and expansion is assumed to be purely linear and happen only in the x-axis. The thermal expansion is therefore modeled as the linear expansion,

$$\Delta l = \alpha L \Delta T ,$$

where α is the coefficient of linear expansion of the material, L is the length of the alignment bar, ΔT is the change in temperature from the reference level, and Δl is the resulting change in length of the bar.

Referring back to Figure 11, the length of the spring corresponds to the length of the alignment bar. Consider a small change in temperature. The alignment bar will have a length of $L + \alpha L \Delta T$ if it is unconstrained. We are, however, hypothesizing a constraining force due to friction, so the bar will actually be compressed. It will be compressed to length $\left(L + \alpha L \Delta T \right) - \Delta x$. The difference Δx being the amount the bar is compressed. The force exerted by the end of the bar is then determined by Hooke's law,

$$F_s = \kappa \left[\left(L + \alpha L \Delta T \right) - \Delta x \right]$$

If we define the origin to be at the right side of the bar at the reference temperature, we can write,

$$F_s = \kappa \left[\alpha L \Delta T - x \right].$$

To understand this, imagine the alignment bar with its right side at $x = 0$. Its left side is constrained at $x = -L$, by a gimbal, and the spring is relaxed. If the temperature rises, the term $\alpha L \Delta T$ becomes non-zero. There is a spring force of $\kappa \alpha L \Delta T$ generated by the alignment bar. This force wants to push the mass to the right, and the system out of equilibrium. As the alignment bar is able to overcome the opposing force (friction or viscous damping), the sprint moves, the difference between its endpoint and its "natural length" decreases and the spring force dissipates. Eventually the spring becomes fully relaxed at its new length, leaving the system in equilibrium.

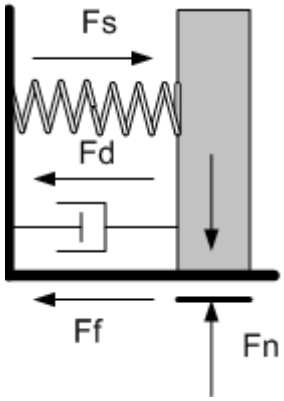

Figure 18: Free Body Diagram with a Pushing Spring Force

If we look at the free-body diagram in this slightly different way (see Figure 18), we see that we need to make a small change to the statement of Newton's second law, since we are expecting the spring to be pushing to the right,

$$m\frac{d^2x}{dx^2} = \kappa x - \zeta\frac{dx}{dt} - \mu_k N \cdot \text{sgn}\left(\frac{dx}{dt}\right).$$

This means we need to write,

$$m\frac{d^2x}{dx^2} - \kappa\left(\alpha L\Delta T - x\right) + \zeta\frac{dx}{dt} + \mu_k N \cdot \text{sgn}\left(\frac{dx}{dt}\right) = f\left(t\right).$$

Now, we would like to have the temperature function be the forcing function, so we need to move it over to the right side,

$$m\frac{d^2x}{dx^2} + \kappa x + \zeta\frac{dx}{dt} + \mu_k N \cdot \text{sgn}\left(\frac{dx}{dt}\right) = \kappa\alpha L\Delta T\ .$$

If we rearrange to the standard form, we arrive at the equation of motion we will use for the alignment bar model, Equation (2):

$$m\frac{d^2x}{dx^2} + \zeta\frac{dx}{dt} + \kappa x = \kappa\alpha L\Delta T - \mu_k N \cdot \text{sgn}\left(\frac{dx}{dt}\right). \qquad (2)$$

7. QUALITATIVE INTERPRETATION OF RESULTS

I began with some qualitative investigations into the general behavior of the model.

First, I asked the question, "What would happen if the alignment bar simply expanded forever against a viscous drag." To answer, I set ΔT to be an increasing function of time (t^2) and set the tunable parameters to $\zeta = 1, \mu_k = 0, \kappa = 1, f(t) = \kappa t^2$. This created a viscously damped harmonic oscillator driven by the thermal expansion of the spring (the alignment bar). I solved Equation (2) in Maple with unit mass.

The results of the solution of the model by Maple are shown in Figure 19. A plot of the forcing function and the response is shown in Figure 20. Consider what is happening in Figure 20. The forcing function is shown in red. This can be thought of as where the length of the bar *would be* if it were unconstrained. As the temperature rises, the unconstrained length of the bar increases. As the speed of the end of the bar increases, the viscous drag does not allow the end of the bar to move as fast as it would like, and so compresses the spring. The bar is deformed as it compresses.

The result is that as the temperature increases faster and faster, the viscous drag force increases more and more. This compresses the spring more and more, and the two curves in Figure 20 move further and further apart. This behavior is consistent with what one would expect in a real system.

```
> ode:= diff(diff(x(t),t),t) + (zeta)*diff(x(t),t) +
(kappa)*x(t) - mu*N = F(t);
```

$$ode := x(t) + \left(\frac{\partial}{\partial t} x(t)\right) + \left(\frac{\partial^2}{\partial t^2} x(t)\right) = t^2$$

```
> dsolve(ode);
```

$$x(t) = e^{(-1/2\,t)} \sin\left(\frac{1}{2}\sqrt{3}\,t\right) \_C2 + e^{(-1/2\,t)} \cos\left(\frac{1}{2}\sqrt{3}\,t\right) \_C1 + t\,(-2+t)$$

```
> soln := dsolve({ode,x(0)=0, D(x)(0)=0});
```

$$soln := x(t) = \frac{4}{3} e^{(-1/2\,t)} \sin\left(\frac{1}{2}\sqrt{3}\,t\right)\sqrt{3} + t\,(-2+t)$$

Figure 19: Maple Code Corresponding to Exponential Temperature Increase

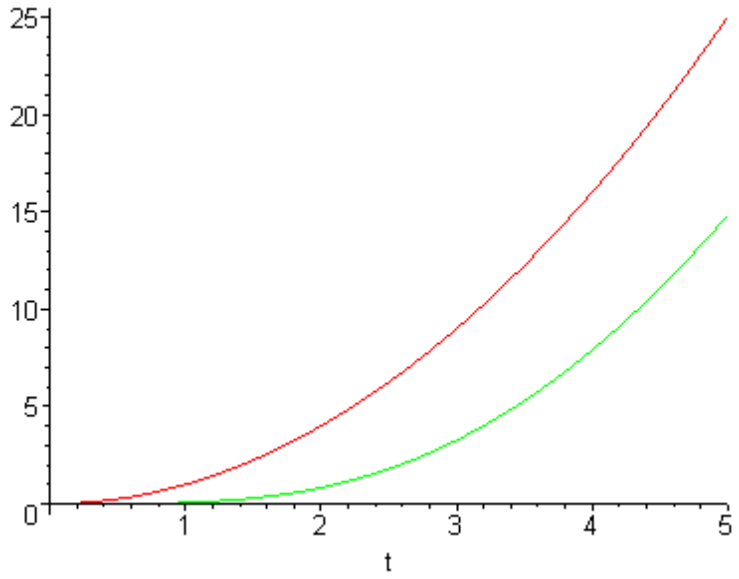

Figure 20: Response of the System to Exponential Temperature Increase

In the next scenario, I asked the question, "What would happen if the alignment bar expanded for a time and then contracted, both against a viscous drag." I made ΔT a piecewise function of time,

$$\Delta T = \begin{cases} t < 0 & 0 \\ 0 < t \le 2\pi & \text{1-cos(t)} \\ 2\pi & 0 \end{cases}.$$

You can see the shape of this function in the red curve of Figure 22. This is a more realistic case, as you can imagine the ambient temperature at the test beam at CERN increasing during the day and then decreasing at night according to a similar function.

I set the tunable parameters to $\zeta = 1, \mu = 0, \kappa = 1$. This created a viscously damped harmonic oscillator driven by the piecewise thermal expansion defined above. I solved the equation of motion, Equation (2). The results are shown in Figure 21. The solutions become quite complicated with the inclusion of the piecewise function.

```
> ode:= diff(diff(x(t),t),t) + (zeta)*diff(x(t),t) +
(kappa)*x(t) + mu*N = F(t);
```

$$ode := \mathrm{x}(t) + \left(\frac{\partial}{\partial t}\mathrm{x}(t)\right) + \left(\frac{\partial^2}{\partial t^2}\mathrm{x}(t)\right) = \begin{cases} 0 & t < 0 \\ 1-\cos(t) & t \le 2\pi \\ 0 & 2\pi < t \end{cases}$$

```
> dsolve(ode);
```

$$\mathrm{x}(t) = \{\, \mathbf{e}^{(-1/2\,t)} \sin\left(\frac{1}{2}\sqrt{3}\,t\right) \_C2 + \mathbf{e}^{(-1/2\,t)} \cos\left(\frac{1}{2}\sqrt{3}\,t\right) \_C1 \,,\ t < 0$$

$$\mathbf{e}^{(-1/2\,t)} \sin\left(\frac{1}{2}\sqrt{3}\,t\right) \_C2 + \mathbf{e}^{(-1/2\,t)} \cos\left(\frac{1}{2}\sqrt{3}\,t\right) \_C1 + \frac{1}{3}\mathbf{e}^{(-1/2\,t)} \sin\left(\frac{1}{2}\sqrt{3}\,t\right)\sqrt{3}$$

$$-\mathbf{e}^{(-1/2\,t)} \cos\left(\frac{1}{2}\sqrt{3}\,t\right) - \sin(t) + 1 \,,\ t < 2\pi$$

$$\mathbf{e}^{(-1/2\,t)} \sin\left(\frac{1}{2}\sqrt{3}\,t\right) \_C2 + \mathbf{e}^{(-1/2\,t)} \cos\left(\frac{1}{2}\sqrt{3}\,t\right) \_C1$$

$$+\frac{1}{3}\sqrt{3}\,\sin\left(-\frac{1}{2}\sqrt{3}\,t + \sqrt{3}\,\pi\right)\mathbf{e}^{(-1/2\,t+\pi)} + \cos\left(-\frac{1}{2}\sqrt{3}\,t + \sqrt{3}\,\pi\right)\mathbf{e}^{(-1/2\,t+\pi)}$$

$$+\frac{1}{3}\mathbf{e}^{(-1/2\,t)} \sin\left(\frac{1}{2}\sqrt{3}\,t\right)\sqrt{3} - \mathbf{e}^{(-1/2\,t)} \cos\left(\frac{1}{2}\sqrt{3}\,t\right),\ 2\pi \le t$$

```
> soln := dsolve({ode,x(0)=0, D(x)(0)=0});
```

$$soln := \mathrm{x}(t) = \mathrm{eval}\Big(\{\, \mathbf{e}^{(-1/2\,t)} \sin\left(\frac{1}{2}\sqrt{3}\,t\right) \_C2 + \mathbf{e}^{(-1/2\,t)} \cos\left(\frac{1}{2}\sqrt{3}\,t\right) \_C1 \,,\ t < 0$$

$$\mathbf{e}^{(-1/2\,t)} \sin\left(\frac{1}{2}\sqrt{3}\,t\right) \_C2 + \mathbf{e}^{(-1/2\,t)} \cos\left(\frac{1}{2}\sqrt{3}\,t\right) \_C1 + \frac{1}{3}\mathbf{e}^{(-1/2\,t)} \sin\left(\frac{1}{2}\sqrt{3}\,t\right)\sqrt{3}$$

$$-\mathbf{e}^{(-1/2\,t)} \cos\left(\frac{1}{2}\sqrt{3}\,t\right) - \sin(t) + 1 \,,\ t < 2\pi$$

$$\mathbf{e}^{(-1/2\,t)} \sin\left(\frac{1}{2}\sqrt{3}\,t\right) \_C2 + \mathbf{e}^{(-1/2\,t)} \cos\left(\frac{1}{2}\sqrt{3}\,t\right) \_C1$$

$$+\frac{1}{3}\sqrt{3}\,\sin\left(-\frac{1}{2}\sqrt{3}\,t + \sqrt{3}\,\pi\right)\mathbf{e}^{(-1/2\,t+\pi)} + \cos\left(-\frac{1}{2}\sqrt{3}\,t + \sqrt{3}\,\pi\right)\mathbf{e}^{(-1/2\,t+\pi)}$$

$$+\frac{1}{3}\mathbf{e}^{(-1/2\,t)} \sin\left(\frac{1}{2}\sqrt{3}\,t\right)\sqrt{3} - \mathbf{e}^{(-1/2\,t)} \cos\left(\frac{1}{2}\sqrt{3}\,t\right),\ 2\pi \le t,\ \{\_C1 = 0, \_C2 = 0\}\Big)$$

Figure 21: Maple Code Corresponding to Piecewise Temperature Increase

A plot of the piecewise function (in red) and the position function of the right side of the alignment bar (in green) is shown in Figure 22. This plot is interpreted as follows: The temperature begins increasing and the alignment bar wants to expand. As the velocity of expansion increases, the expansion is resisted by the viscous drag and the alignment bar compresses. The amount of compression manifests itself as the difference in the amplitudes of the curves at a particular time.

As the rate of temperature increase reaches its maximum value, the bar is compressed by an amount proportional to the viscous drag force. This continues and the temperature increase slows and eventually reverses. At the time the temperature peaks and begins going down, the spring is relaxing and releasing its stored energy. This moves the end of the alignment bar out to its fully extended length, which is the same length as the maximum of the forcing function; but which happens at a later time. The situation is reversed as the bar shrinks with temperature decrease and pulls against the viscous drag that wants to keep it extended. As the bar comes back down to $\Delta T = 0$, the bar overshoots slightly and then undergoes a damped oscillation until it reaches equilibrium.

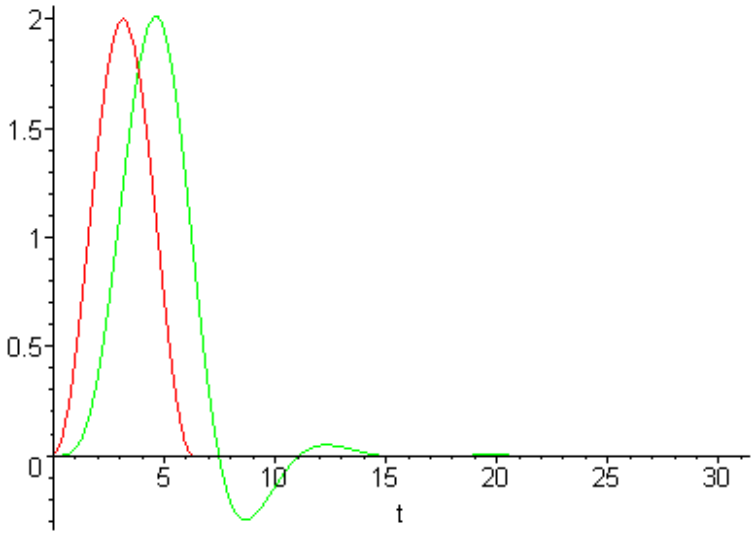

Figure 22: Response of the System to Piecewise Temperature Increase

The model seems to accurately reflect the physics involved.

Next, I modeled the distortion one would see on an alignment bar during the compression and tension phases of the last test. I did this by subtracting the response curve from the forcing curve. This is a measure of the energy stored in the spring and is shown by the blue curve in Figure 23.

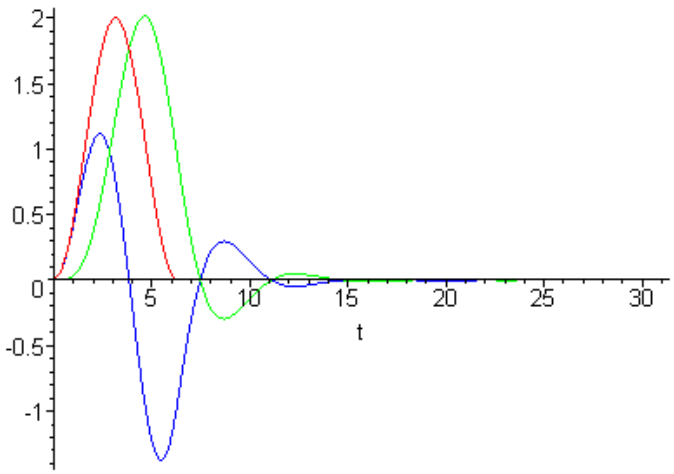

Figure 23: Qualitative Representation of the Distortion of the Alignment Bar Due to the Piecewise Temperature Increase

Springs change shape when they are compressed or extended. The alignment bar will do so as well. Due to the torque imposed by the loose bearing, when the alignment bar is compressed due to the friction of the bearing, it will tend to bow upward. Conversely, when the bar is extended, the torque will cause it to bow downward.

Figure 24 shows a zoom into a section of Figure 23 in which the distortion measure has been changed slightly – the sign of the distortion has been changed, and a constant offset has been added. The red curve is the forcing function and the blue curve is the qualitative alignment bar distortion. The reason for these changes will be clear if you compare Figure 10 and Figure 24. The justification for the change is that the RasNik measurement devices located in the alignment bars measure a bow upward with a decrease in position measurement – this corresponds to the inversion of the curve. There is also a nonzero value for the RasNik at equilibrium which corresponds to the addition of a fixed offset.

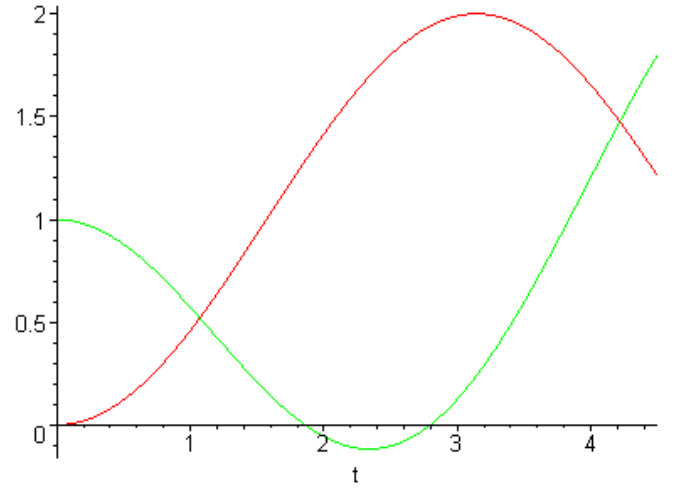

Figure 24: Qualitative Representation of the Distortion of the Alignment Bar

As a result, Figure 24 is a simulation of what a RasNik device might report as a result of the forcing function. The qualitative similarity between Figure 24 (the results of the simulation with a qualitative view of distortion) and Figure 10 (actual alignment bar data from CERN) is unmistakable. Both figures are reproduced below for closer inspection.

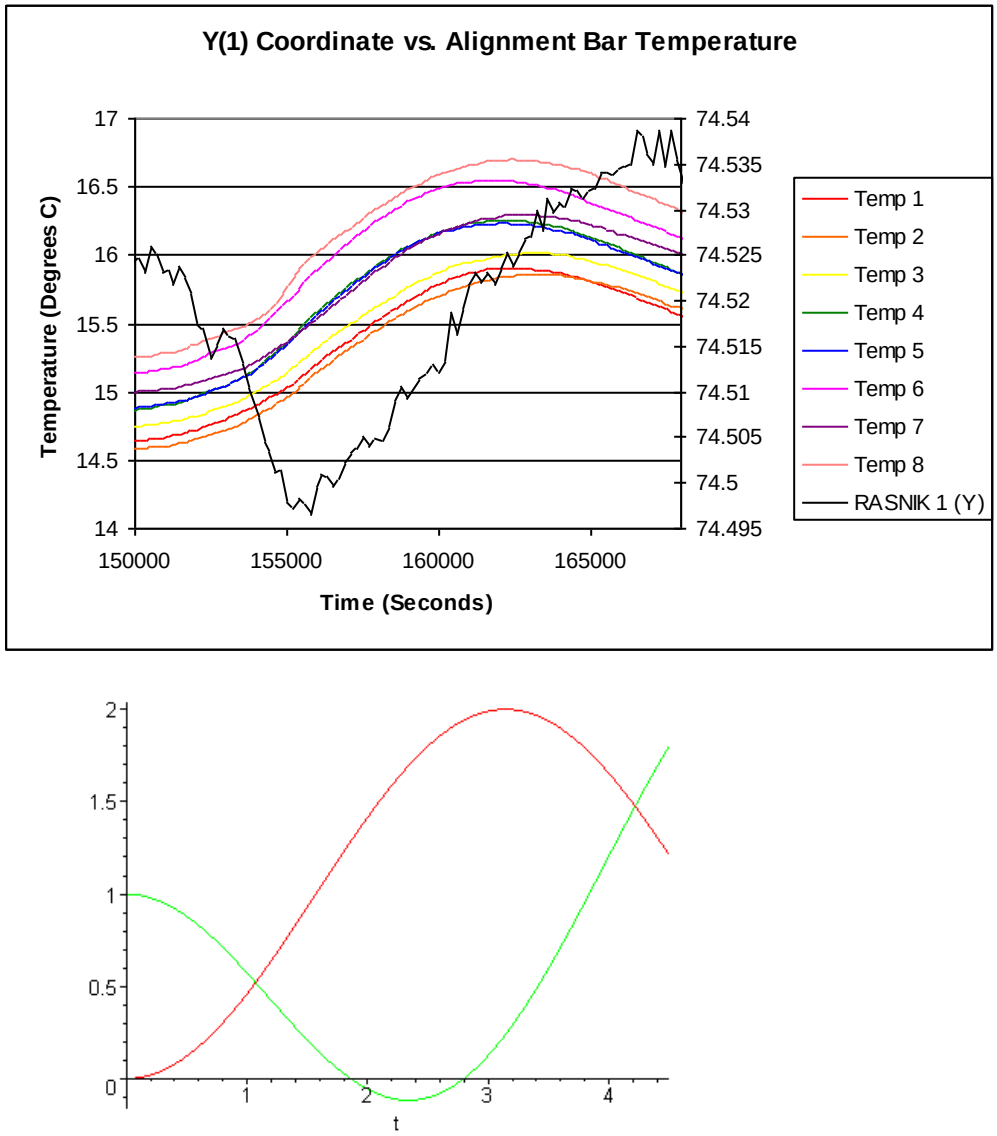

Figure 25: Upper: Measured Distortion of the Alignment Bar Due to Temperature Increase; Lower: Predicted Qualitative Distortion due to Temperature Increase

8. QUANTITATIVE INTERPRETATION OF RESULTS

The qualitative results of the previous section showed that a combination of forces such as those reflecting a restoring force and a damping force could be combined to produce the results seen at the test beam at CERN. This does not, however, tell us that the actual combination of forces seen at the test beam would produce such a result in the model. In order to determine whether this would be the case, I adjusted the model parameters to reflect the physical setup at CERN.

I determined the values of the parameters based on information in the design and test documentation of the alignment bar. The weight of the alignment bar is 60 pounds, supported at two points. This means that each support on a horizontally mounted bar will support 30 pounds, or roughly 14 kilograms. This is the value for N, the normal force in the model. The coefficient of linear thermal expansion is given as $23.8\times10^{-6} mK^{-1}m^{-1}$, which becomes the parameter α in the model. The length of the long alignment bar is 960 mm, which becomes the parameter L. The cross sectional area A is derived from the outer and inner diameters of the alignment bar tube:

$$A=\pi\left(\frac{0.085}{2}\right)^2-\pi\left(\frac{0.077}{2}\right)^2.$$

Young's modulus for aluminum fixes the parameter $E=70\times10^9$, and the spring constant is derived from Young's modulus:

$$\kappa=\frac{EA}{L}$$

The forcing function of the model is defined as:

$$f(t)=\kappa\alpha L\delta,$$

where δ is the function describing the change in temperature.

The remaining parameters are the coefficient of kinetic Coulombic friction, μ, and the coefficient of viscous damping, ζ. Table 1 shows a selection of known coefficients of Coulombic friction

.

Materials	μ_k
Wood on Wood	0.2
Ice on Ice	0.03
Metal on metal (lubricated)	0.06
Steel on steel (unlubricated)	0.6
Rubber on Dry Concrete	0.8
Rubber on Wet Concrete	0.5
Teflon on Steel in Air	0.04

Table 1: Selection of Coefficeints of Kinetic Friction

These parameters were entered into Maple and the coefficient of kinetic Coulomb friction was varied in a system driven by a piecewise time function chosen to approximate the temperature measurements in the CERN data which rose by about 1.6 degrees K in 90 minutes (5400 seconds)

$$\delta = 1.6\begin{cases} t < 0 & 0 \\ t \geq 0 & 1-\cos\left(\pi/5400\, t\right) \end{cases}.$$

As a reference, the system's response was compared to a case of zero coulomb friction.

Figure 26 shows the results of a simulation run with the red curve being zero friction, and the green curve having $\mu = 0.6$ which represents unlubricated steel on steel. The vertical scale is measured in meters, and so 0.0002 corresponds to 200 μm. If you look very closely, you can see tiny bits of green, indicating a tiny difference between the curves. This indicates an even smaller bow in the alignment bar, which is nowhere near the 30 μm displacement we saw in the CERN data, which would be a distortion of over a ½ minor division separation at the scale of the figure.

Figure 27 shows the results of a run with $\mu = 1.0$. Again, the simulated bow in the alignment bar is nowhere near the value seen in the CERN data. This leads me to believe that the normal force causing the friction cannot be due to gravity.

If we leave the coefficient at $\mu = 1.0$, and increase the normal force beyond mg, we expect that the curves will separate further and further. This is expected, since the friction force has the effect of compressing the spring by a *constant* amount proportional to the normal force. It is important to note, however, that Coulomb friction alone cannot explain the behavior which is correlated with the derivative of time. We need to invoke viscous damping to explain that.

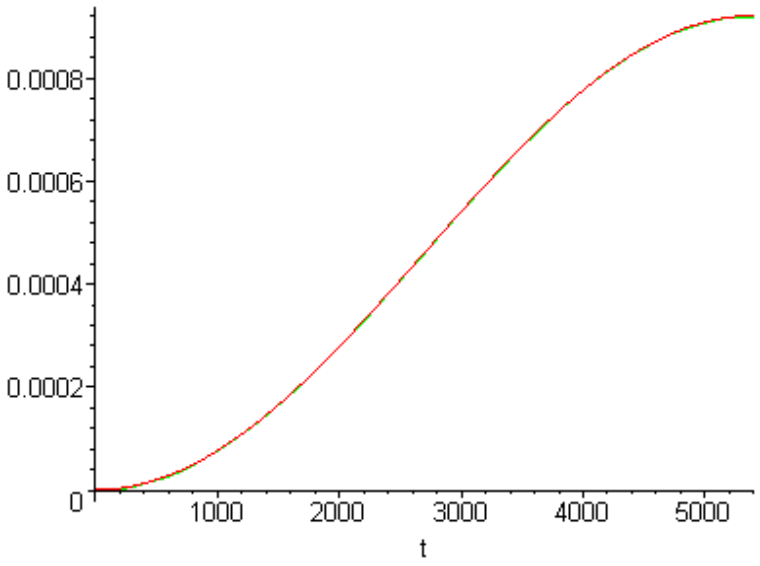

Figure 26: Expected Distortion of the Alignment Bar μ=0.6

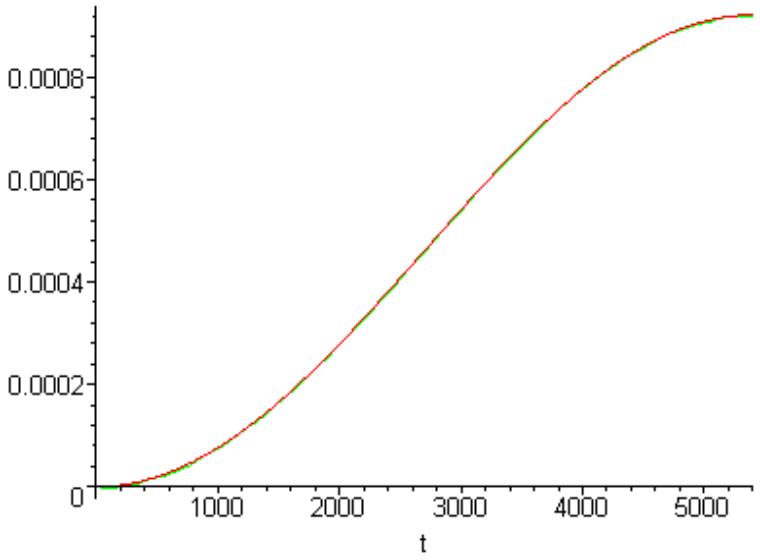

Figure 27: Expected Distortion of the Alignment Bar at μ=1.0

Figure 28 shows a simulation run in which the curve of position of the end a bar constrained by viscous damping (green) separates from the curve of the unconstrained position by roughly the amount seen in the CERN data.

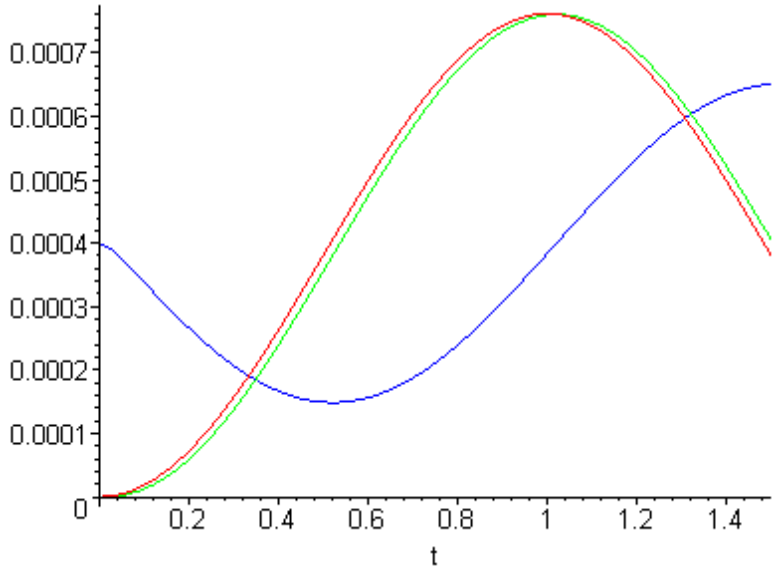

Figure 28: Extreme Conditions Required for a Distortion

The blue curve is the difference between the red curve and the green curve, shifted up from 0 to 0.0004 and multiplied by a constant scale factor of -10. This is the equivalent of what was done in Figure 24, but the simulation is now using physical values of the tunable parameters.

Notice that in order to reproduce the CERN data, the time scale has been decreased, with respect to Figure 27, by a factor of 5400. This would represent a change in temperature of over 1.5 K per second in the test beam environment. The coefficient of viscous damping required a level of 150 000 in order to obtain this result. This environment is wildly inconsistent with the actual environment at CERN, where the temperature changed roughly 1.5 K over 90 minutes; and it is hard to imagine the mechanism that would provide a viscous damping constant of 150 000, outside of a structural seismic viscous damper.

9. CONCLUSION

The shape of the distortion of the alignment bars due to over excursions in temperature is shown, in principle, to be explainable by drag forces and torques on the alignment bar. The behavior is not explainable by Coulomb friction alone as was implied by the original hypothesis. Coulomb friction will introduce a constant distortion once static friction is overcome. A viscous drag mechanism must be invoked to reproduce the behavior dependent on the inverse derivative of temperature seen at the CERN test beam.

We can construct simulations that qualitatively and quantitatively compare favorably with the CERN data (see Figure 24, Figure 26). In order to do so, however, the changes in ambient temperature and the drag forces required are ridiculously above possible real values for physical constants and rates of change that could be found in a real system.

I conclude that the anomalous measurements at the test beam can not be due to friction and torque as surmised, but are due to another unrelated mechanism.

Refereneces

[1] Boyce, W., DiPrima, R., *Elementary Differential Equations*, John Wiley and Sons, New York (2003)

[2] Craig, R., *Structural Dynamics*, John Wiley and Sons, New York (1981)

[3] Giancoli, D., *Physics for Scientists and Engineers*, Prentice Hall, Upper Saddle River, (2000)

[4] Haberman, R., Mathematical Models, Society for Industrial and Applied Mathematics, Philadelphia (1998)

[5] Reskick, et. al., Physics Volume 1, John Wiley and Sons, New York (2002)

[6] Schricker, A., *The Alignment System of the ATLAS Muon End-Cap Spectrometer*, <http://atlas.web.cern.ch/Atlas/documentation/thesis/schricker/thesis.pdf>

[7] Van der Graaf, et. al., *RasNiK, an Alignment System for the ATLAS MDT Barrel Muon Chambers Technical System Description*, <http://atlas.web.cern.ch/ Atlas/ GROUPS/MUON/alignment/documents/RasNiK_Note_Rev2.pdf>